(3) Rouse, P. *J. Chem. Phys.* **1953**, *21*, 1272.
(4) de Gennes, P.-G. *Scaling Concepts in Polymer Physics*: Cornell University Press: Ithaca, NY, 1979.
(5) Cohen-Addad, J. P.; Dupeyre, R. *Polymer* **1983**, *24*, 400.
(6) Cohen-Addad, J. P.; Guillermo, J. *J. Polym. Sci.* **1984**, *22*, 931.
(7) Cohen-Addad, J. P. *J. Phys. (Les Ulis, Fr.)* **1982**, *43*, 1509.
(8) Cohen-Addad, J. P.; Domard, M. *J. Chem. Phys.* **1982**, *76*, 2744.
(9) Cohen-Addad, J. P.; Boileau, S. *J. Chem. Phys.* **1981**, *75*, 4107.
(10) Doi, M.; Edwards, S. F. *The Theory of Polymer Dynamics*; Clarendon Press: Oxford, 1986.
(11) Ullman, R. *J. Chem. Phys.* **1965**, *43*, 3161.
(12) Geschke, D.; Poschel, K. *Colloid Polym. Sci.* **1986**, *264*, 482.
(13) Muller, K.; Schleicher, A.; Ohmes, E.; Ferrarini, A.; Kothe, G. *Macromolecules* **1987**, *20*, 2761.
(14) Rossler, E.; Sillescu, H.; Spiess, H. W. *Polymer* **1985**, *26*, 203.
(15) Kimmich, R.; *Prog. Nucl. Magn. Reson. Spectros.* *20*, **1988**, 385.
(16) McCall, D.; Douglass, D.; Anderson, E. *J. Polym. Sci.* **1962**, *59*, 301.
(17) Kimmich, R.; Bachus, R. *Colloid Polym. Sci.* **1982**, *260*, 911.
(18) Wright, P. Thesis, University of Leeds, 1988.

Correlation of Phase-Separation Behavior in Polymer Blends with Thermodynamic Measurements in the One-Phase Region

J. S. Higgins,* H. Fruitwala, and P. E. Tomlins

Department of Chemical Engineering and Chemical Technology, Imperial College, London SW7 2BY, England. *Received August 29, 1988; Revised Manuscript Received February 1, 1989*

ABSTRACT: When a polymer blend is heated to within the unstable region of the temperature composition diagram, spinodal decomposition may be observed using small-angle neutron scattering. In the one-phase region, scattering has been used to obtain the temperature and composition dependence of the second derivative with respect to composition of the Gibbs free energy of mixing. Correlation of these two types of measurements not only tests the current theories of spinodal decomposition but also provides insight into the molecular parameters controlling domain morphology in phase-separating blends.

Introduction

If the temperature of a partially miscible polymer blend is raised from the one-phase region to the two-phase region, then concentration fluctuations become unstable, and phase separation results via spinodal decomposition.[1,2] The driving force for this process is provided by the gradient of the chemical potential.[3] There has been a recent surge of interest in the theory[4-7] and the experimental observation[8-10] of phase separation in polymer blends both because of the technological interest in polymeric materials and because the high viscosities of these systems slow down the process and allow the kinetics in the early stages to be observed and thus test the theoretical predictions.

For the most commonly studied system—polystyrene with poly(vinyl methyl ether)—the wavelength of the unstable concentration fluctuations lies dominantly around 10^4 Å, and therefore light-scattering techniques have been employed. Recently, Meier and Strobl[11] employed SAXS to study a blend of polystyrene with poly(styrene-*co*-bromostyrene) well away from the dominant distance scale. However, for a number of systems, we have noted length scales of less than 10^3 Å in the scattering from two-phase blends. An example of such a system is poly(methyl methacrylate) with solution chlorinated polyethylene,[12] and in this case SANS and SAXS techniques were the obvious choices of scattering techniques.

In several recent papers[13-19] it has been shown that small-angle neutron-scattering measurements from the concentration fluctuations in a single-phase two-component polymer blend may be used to determine the Flory interaction parameter of the blend. The concentration fluctuations in such a system were originally shown by Einstein[20] to depend on the concentration gradient of the chemical potential, which Debye and Bueche[21] subsequently related to interactions in the system using the Flory–Huggins equation.[22]

If the temperature and concentration dependences of the chemical potential gradient are determined, then, by extrapolation, it is possible to obtain values inside the phase boundary and thus to predict the dominant length scale for phase separation. In this paper we test, for the first time, this correlation between neutron scattering from the stable and unstable regimes of the phase diagram for a blend of poly(methyl methacrylate) (PMMA) with poly(α-methylstyrene-*co*-acrylonitrile) (PAMSAN).

The linearized theory of spinodal decomposition was originally developed for small-molecule systems by Cahn and Hilliard,[1,2] subsequently adapted to polymeric systems by van Aartsen,[3] and reformulated on the basis of mean-field theory to predict the behavior of the intensity of scattered radiation as function of time by Pincus,[4] de Gennes,[5] and most extensively by Binder.[6]

The influence of thermal fluctuations was first introduced to the theoretical development by Cook,[23] and the significance was further explored by Binder.[24] Okada and Han[10] showed that the contribution to the observed scattering from thermal fluctuations was negligible except when experiments were carried out very close to the spinodal temperature (in this case, "very close" meant within 1°). The small-angle neutron-scattering data from blends of PMMA/PAMSAN presented in this paper are used to test the theoretical predictions; for spinodal decomposition, in particular, the influence of thermal fluctuations near the spinodal temperature is examined in some detail.

Thermodynamics of Polymer Blends

The free energy of mixing, ΔG_m for a polymer blend may be calculated from the Flory–Huggins lattice model.[22] ΔG_m is here expressed per lattice segment and

$$\Delta G_m/RT = n_1 \ln \Phi_1 + n_2 \ln \Phi_2 + \Phi_1\Phi_2\chi_{12} \quad (1)$$

n_1 and n_2 are the molar numbers of polymers 1 and 2, respectively. Φ_1 and Φ_2 are the volume fractions of the components. χ_{12} is the interaction parameter. In the original Flory–Huggins theory[22] χ_{12} was independent of concentration and inversely dependent on temperature. However, with such a simple description of χ_{12} eq 1 is

0024-9297/89/2222-3674$01.50/0

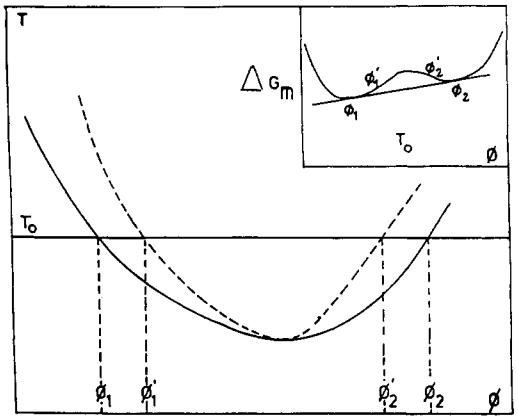

Figure 1. Hypothetical phase diagram of a polymer mixture exhibiting an LCST.

unable to predict the behavior of most real polymer systems. Either more complex equation of state formulations[25,26] of ΔG_m must be invoked or eq 1 is used but with an empirical temperature and concentration-dependent χ_{12}.

The inset in Figure 1 is a typical dependence of ΔG_m on Φ for a system that is partially miscible at the temperature of observation, T_o. The main diagram in Figure 1 shows the corresponding miscibility limits in temperature and composition. Clearly, for any composition between Φ_1 and Φ_2 the system can reduce ΔG_m by separating into two phases with composition Φ_1 and Φ_2. The solid line in Figure 1 is called the binodal and is defined by the points of common tangent to ΔG_m (i.e. Φ_1 and Φ_2 at T_0). At these compositions the chemical potentials μ_1 and μ_2 are equal and the two phases can coexist.

The dashed line is the spinodal, defined by the points of inflection where $\partial^2/\partial\phi^2(\Delta G_m) = 0$. These points are Φ_1' and Φ_2' in the inset. For compositions between Φ_1' and Φ_2', $\partial^2/\partial\phi^2(\Delta G_m) < 0$ and the system is unstable to all small concentration fluctuations. The phase-separation process is called spinodal decomposition. Between Φ_1 and Φ_1' and Φ_2' and Φ_2, $\partial^2/\partial\phi^2(\Delta G_m) > 0$ so that small fluctuations are damped out and phase separation proceeds by a nucleation and growth process. For $\Phi < \Phi_1$ and $\Phi > \Phi_2$ the system is a stable single phase. The point where the binodal and spinodal meet is the critical point.

Two points are worth noting. First, the phase diagram is inverted compared to similar ones for low molecular weight systems. This is typical of high molecular weight polymer blends and arises because of the relative unimportance of the combinational entropy of mixing (the first two terms in eq 1 become very small as n_1 and n_2 become small). Second, the diagram is not symmetrical. This again is typical and usually suggests $n_1 \neq n_2$ but may also indicate a complex variation of χ with Φ.

It is the second derivative of ΔG_m with respect to Φ that governs both the intensity of scattering in the single phase outside the binodal and the kinetics of phase separation inside the spinodal.

From eq 1 we obtain

$$\partial^2/\partial\phi^2(\Delta G_m/RT) = (N_1\Phi_1)^{-1} + (N_2\Phi_2)^{-1} - 2\chi_{12} \quad (2)$$

Here N_1 and N_2 are the number of lattice sites occupied by polymers 1 and 2 (given by the degree of polymerization if the lattice site is assumed to be occupied by a monomer of either polymer). If χ_{12} is concentration dependent, then its concentration gradient will also appear. Since the second derivative in eq 2 appears frequently throughout this paper, we have adopted a shorthand notation $G'' \equiv \partial^2/\partial\phi^2(\Delta G_m/RT)$.

Small-Angle Scattering from Polymer Blends

On the basis of mean-field theory (or the so-called random-phase approximation), it has been shown by a number of authors[13,17,18] that normalized scattering per segment volume from a two-component system may be approximated to

$$S_T^{-1}(Q) = S^{-1}(0)[1 + Q^2R_{ap}^2/3] \quad (3)$$

where

$$S^{-1}(0) = (N_1\Phi_1)^{-1} + (N_2\Phi_2)^{-2} - 2\chi_{12} \quad (4)$$

$Q = (4\pi/\lambda)\sin(\theta/2)$, and R_{ap} is a function of both the radii of gyration of the component polymers and of χ_{12}.

$$R_{ap}^2 = \left[\frac{R_{g_1}^2}{\Phi_1 N_1} + \frac{R_{g_2}^2}{\Phi_2 N_2}\right] S(0) \quad (5)$$

Analysis of SANS data in terms of eq 4 involves either extracting $S^{-1}(0)$[14-16,19] from the normalized forward scattered intensity or choosing the best value of χ_{12} to fit the observed values of R_{ap} as a function of Φ.[17-19] The problem with this latter approach is its requirement for values of both the radii of gyration and degree of polymerization of the component polymers. Very careful normalization of the data is required in order to obtain reliable values of $S^{-1}(0)$, and particular attention must be paid to subtraction of incoherent scattering backgrounds.

Spinodal Decomposition

Cahn and Hilliard[1,2] derived a diffusion equation for a spinodal decomposition process

$$-\partial\phi/\partial t = MG''\nabla^2\Phi - 2MK\nabla^4\Phi + \text{nonlinear terms} \quad (6)$$

M is the diffusional mobility of the system and the term K arises from the free energy in the concentration gradients. K is determined by the statistical segment lengths of the component polymers.[7]

The mobility term M has been the subject of considerable recent discussion.[27,28] While it evidently is governed by the mutual diffusion coefficients D_1 and D_2 of the component polymers, the exact method of combination of D_1 and D_2 and the modification of each in the presence of the other polymer are not clear.

Equation 6 can be solved (if nonlinear terms are ignored) in terms of growth $R(Q)$ in amplitude of each Fourier component of the concentration fluctuations.

$$R(Q) = -MG''Q^2 - 2MKQ^4 \quad (7)$$

The function has a maximum at

$$Q_m = \tfrac{1}{2}[G''/K]^{1/2} \quad (8)$$

and for values of $Q > Q_c = 2^{1/2}Q_m$, $R(Q)$ becomes negative so that short wavelength fluctuations are damped out.

The scattered intensity from such a system grows exponentially with time as

$$S(Q,t) = S(Q,0)\exp[2R(Q)t] \quad (9)$$

where $R(Q)$ is given by eq 7. The coefficient of the first term on the right-hand side of eq 6 is identified as the Cahn–Hilliard diffusion coefficient, $\bar{D}$.

$$\bar{D} = M(-G'') = -2R(Q_m)/Q_m^2 \quad (10)$$

The early stages of spinodal decomposition (where G'' does not differ too strongly from its initial value) are observed as an exponentially increasing scattered intensity, which develops a maximum at Q_m. During the early stages Q_m

is not time dependent and so the maximum remains at constant Q. $\bar{D}$ can be obtained from the intercept of a plot of $R(Q)/Q^2$ vs Q^2 following eq 7. These values extrapolate to zero at the spinodal temperature where $G'' = 0$.

Extraction of the free energy term from eq 7 requires knowledge of M or K. Alternatively, values of G'' can be extrapolated from the one-phase region and then used to check the theoretical predictions for K or to obtain the concentration dependence of M.

Equation 9, on which the analysis of $R(Q)$ is based, is actually a simplification because it omits the effect of thermal fluctuations in the system.

While the effect of thermal fluctuations was originally developed using the Cahn–Hilliard formalism, for convenience we follow Binder,[4] Strobl,[29] and Pincus[6] and rewrite eq 6 in terms of the random-phase approximation including the thermal fluctuation term to obtain

$$\partial/\partial t(S(Q,t)) = 2MQ^2(S_T^{-1}(Q)S(Q,t) - 1) \quad (11)$$

$S_T(Q)$ is as defined in eq 3, but since G'' is negative inside the spinodal, $S_T(Q)$ will be negative for part of the Q range and therefore not observable experimentally. The solution of eq 11 is

$$S(Q,t) = \{S(Q,0) - S_T(Q)\}e^{2R(Q)t} + S_T(Q) \quad (12)$$

where

$$R(Q) = -MQ^2S_T^{-1}(Q) \quad (13)$$

and substituting from eq 3–5, we find

$$R(Q) = -MQ^2\left\{G'' + \left[\frac{R_g^2{}_1}{\Phi_1 N_1} + \frac{R_g^2{}_2}{\Phi_2 N_2}\right]\frac{Q^2}{3}\right\} \quad (14)$$

Comparison with eq 7 now allows us to identify K.

$$K = \tfrac{1}{6}\left\{\frac{R_g^2{}_1}{\Phi_1 N_1} + \frac{R_g^2{}_2}{\Phi_2 N_2}\right\} \quad (15)$$

Given that the ratio R_g^2/M_w is quoted for a number of bulk polymers and ignoring complications such as polydispersity effects or changes in conformation in the blend, we write

$$K = \frac{m_1}{6}\left[\frac{(R_g^2/M_w)_1}{\Phi_1} + \frac{(R_g^2/M_w)_2}{\Phi_2}\frac{m_2}{m_1}\right] \quad (16)$$

where m_1 and m_2 are monomer masses of the two polymers.

Since G'' can be determined by temperature extrapolation from the one-phase region and since K and M can in principle be determined from properties of the homopolymers, the only unknown in eq 12 is $S(Q,0)$. Now this is the scattered intensity at time zero, which presumably for an infinitely sharp temperature jump, is the scattered intensity at the temperature before the jump. This is just $S_T(Q)$ again as in eq 3 but with a value of G'' appropriate to this prejump temperature. Since, now, two values of G'' will be necessary parameters, we identify that in the one-phase region (prejump) as G''_i and that in the two-phase region (postjump) as G''_f. Of course, real temperature jumps are not infinitely sharp, and G''_i may reflect a whole range of intermediate temperatures. Binder[30] has explored by computer simulation the effect of "slow" jumps.

The relative importance of the thermal fluctuation term compared to $S(Q,0)$ and the resulting influence on the observed growth rate are discussed in some detail in this paper.

Table I
Sample Characteristics

sample	M_w	M_w/M_n	T_g, °C
PAMSAN	8.47×10^4	2.20	107
PMMA	1.12×10^5	1.75	114

Experimental Section

Samples. The poly(α-methylstyrene-*co*-acrylonitrile) (PAMSAN) random copolymer was obtained from BASF, West Germany (KR2556). The industrial PAMSAN was dissolved in dry methyl ethyl ketone (MEK) and reprecipitated using methanol to remove plasticizers, fillers, or antioxidants. The deuterated poly(methyl methacrylate) (PMMA-*d*) was obtained from du Pont de Nemours and Co. Ltd. Different molecular weight PMMA-*d* was obtained by γ-irradiating in our laboratory for controlled periods of time. This procedure produces samples with a fairly narrow molecular weight distribution and does not induce cross-linking into the specimens.[31] Sample characteristics are noted in Table I.

Blend Preparation. Thin films of the blends were made by evaporating solutions containing known weights of PMMA-*d* and PAMSAN in dry MEK to dryness. The thin films were then placed under vacuum at 80 °C for periods of up to 1 week to ensure removal of all traces of the solvent. Typical film thicknesses were 0.1–0.2 mm.

Determination of Phase Boundary. Prior to any study of real-time kinetics, the cloud-point curve was estimated using a hot-stage microscope (Olympus, BH) in our laboratory. The sample holder was placed under the microscope, and the sample was heated at a rate of 1 °C/min. The cloud point was recorded at a point when the sample went bluish and two phases started appearing. Although the closeness of refractive indices of these two polymers and the small domain sizes observed hindered the accurate measurement of cloud points, these measurements give a good idea of the correct temperature range in which to perform kinetic experiments.

Kinetic Experiments. Kinetic experiments were performed on the small-angle neutron-scattering (SANS) spectrometer D11[32] at the Institute Laue–Langevin (Grenoble, France). A sample-detector distance of 10.0 m was used with neutrons of wavelength 8.01 Å. Correction was made for the detector response using the incoherent scattering from water. Also the data from the area detector were radially averaged over a 2-cm grid.

The experimental procedure followed was to clamp a 12-mm-diameter disk of film into a recess set in a thin brass finger using a narrow ring. This arrangement allowed use of a 10-mm-diameter neutron beam. The brass finger was then inserted into a preheated brass block set at a temperature about 10 °C below that of the phase boundary and allowed to equilibrate for 5–10 min. The finger was then transferred to a second brass block located in the neutron beam, which had been preheated to a temperature above the cloud point (obtained using a hot-stage microscope). The time of insertion into the second block was taken as time zero, and spectra were recorded over 10-s intervals for periods of up to 20 min when the experiment was terminated. The time interval between ending and beginning successive spectra was approximately 4 s, which was accounted for in determining the time scale of the experiment.

SANS from Quenched Samples. The SANS measurements were carried out at room temperature on annealed and quenched samples. Thin disks approximately 16 mm in diameter and about 0.8–1 mm thickness were made by compression-molding stacked thin films of the blend samples originally prepared for kinetic experiments. Each disk of different composition of blend was annealed at temperatures below the cloud point for about 2 h, when they were quenched in cold water. The details of annealing time and temperature for different blend composition are given in Table II. This enabled G'' to be obtained from the forward scattering intensity (eq 2 and 4) as a function of temperature in the one-phase region. The method is described in detail in previous publications.[13–15,19]

The SANS experiments were performed on the D17 spectrometer[33] at the ILL (Grenoble, France) using a sample-detector distance of 3.42 m and neutrons of wavelength 15 Å. The measurements were made of scattering from each polymer sample

Table II
Single-Phase Results

comp (PAMSAN/PMMA)	annealing conditions		$G'' \times 10^3$
	time, min	temp, °C ±0.2	
20/80	120	133.4	5.5
	120	138.7	2.8
26/74	120	123.8	18.1
	120	133.4	12.2
	120	138.7	6.8
	120	145.6	0.18
40/60	120	132.5	20.8
	120	138.5	16.2
	120	145.1	9.6
	120	150.2	6.4

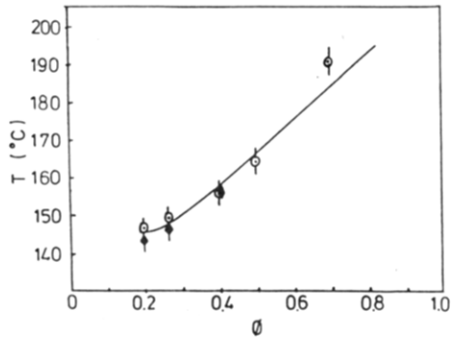

Figure 2. Cloud-point curve obtained on a hot-stage microscope (⊙). ♦ are spinodal temperatures for PAMSAN/dPMMA blends.

(disk), the pure hydrogenous sample, the empty cell holder, a 1-mm-thick water sample, and the empty water cell. Data were normalized for geometric and flux factors using the isotropic incoherent scattering from water. The incoherent background for each sample was removed as described previously in detail.[13-14]

Results

(1) Determination of the Phase Boundary. The cloud-point curve obtained from the hot-stage microscope is shown in Figure 2. As explained earlier phase separation is only detectable by this method in the very late stages, so that the true spinodal may lie below the curve in Figure 2. Since phase separation was well developed and fairly rapid, cooling on removal of the sample from the hot stage, the blend did not remix. Parts a–d of Figure 3 show the development of the phase-separation process for a 26/74 mixture of PAMSAN with PMMA. The typical interconnected structure of the spinodal decomposition process can clearly be seen in Figure 3a. The interconnected structure breaks down with time (parts c and d Figure 3) eventually forming small droplets.

For this blend a more precise value of the spinodal temperature should be obtained by considering the neutron cloud point, i.e. the temperature at which the forward neutron-scattered intensity becomes infinite. Figure 4 shows the intensity scattered by the 26/74 blend annealed at four temperatures. As annealing temperature increases, so does the scattered intensity. From the forward scattered intensity, $S(0)$, values of G'' are obtained directly (eq 3 and 4) and plotted against inverse temperature in the upper part of Figure 5. (An inverse temperature dependence of G'' is expected because of the inverse temperature dependence of χ_{12}.[13-15,19]

The spinodal temperature is the point where $G'' = 0$. However, Figure 5 shows that, given the experimental uncertainty in the data, there remains several degrees of uncertainty in any spinodal temperature obtained in this way. Overall, the points are within 1 or 2 deg of the cloud points determined optically.

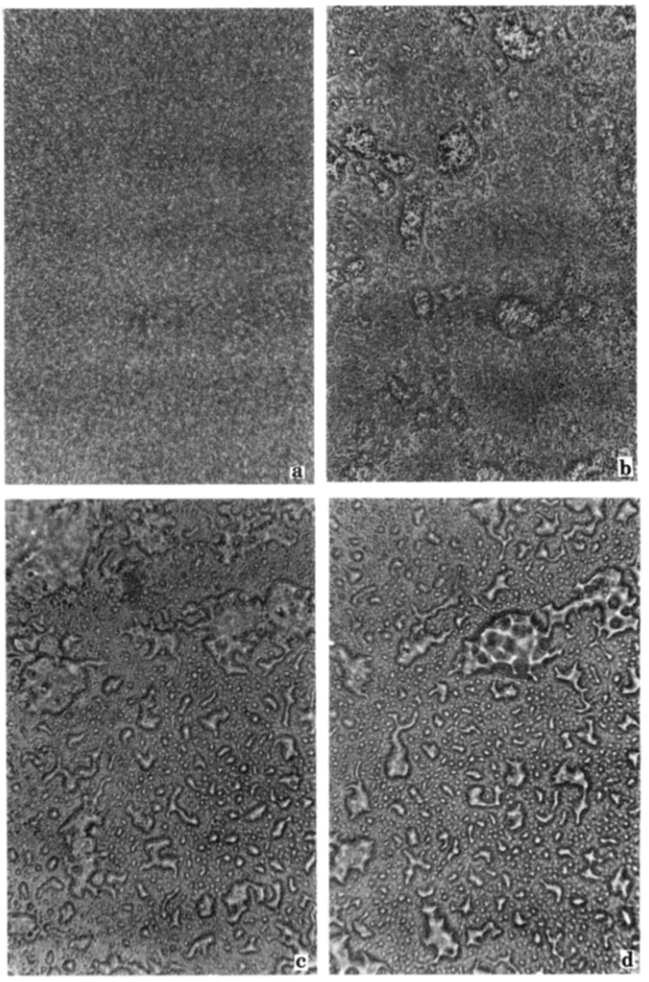

Figure 3. Development of phase separation in blends, as in Figure 2, as seen in the phase contrast microscope. 1 cm = 10 μm.

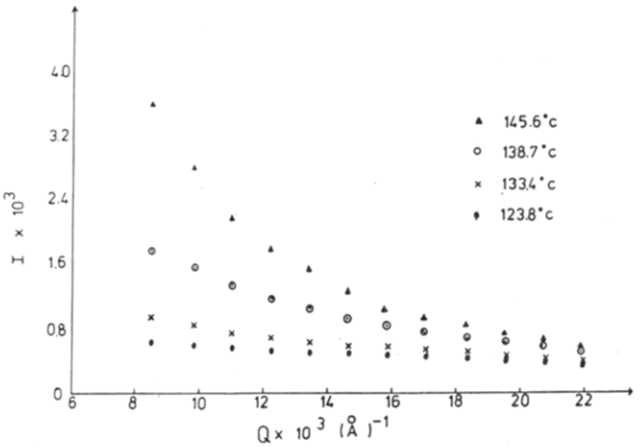

Figure 4. Normalized scattered intensity from a 26/74 blend at temperatures as shown.

(2) Real-Time Kinetic Studies. Figure 6 shows the evolution of the scattered intensity from a 26/74 sample after a temperature jump into the two-phase region. In the early stages intensity increases over the whole Q range, but eventually a maximum appears as predicted by eq 7–9. The growth rate of the intensity is exponential at each Q value in the initial stages and a typically linear plot of ln I vs t is shown in Figure 7. Such linearity is usually taken as a sign that the early stages of spinodal decomposition have been observed and that Cahn–Hilliard theory would be expected to apply. All the kinetic data showed this linearity, implying that eq 9 satisfactorily fits the results

Table III

blend comp	temp, °C	Q_m, $\times 10^3$ Å^{-1}	d_0, Å	$Q' = (1/2)[\text{int/slope}]^{1/2}$, $\times 10^3$ Å^{-1}	K, Å^2	G''_f from Q_m, $\times 10^3$	$\bar{D}$, $\times 10^{19}$ m^2 s^{-1}	M from MK, $\times 10^{16}$ m^2 s^{-1}	ΔT (from G''_f), m^2 s^{-1}
26/74	151.5	9.8	641	12.69		-3.08	14.0	2.71	4
	153.0	11.0	571	11.95	8.01	-3.87	15.2	3.28	5.5
	154.0	11.2	560	11.09		-4.01	15.5	3.93	6.5
	155.0	11.5	546	10.78		-4.24	16.8	4.46	7.5
20/80	149	9.9	634			-3.82	15.4		5.4
	150	10.1	622	11.30	9.74	-3.97	20.5	4.12	6.4
	153	10.5	598	11.44		-4.30	23.8	4.66	9.4
40/60	158.0	10.5	598	10.7	6.27	-2.76	22.2	7.59	1.5
	160.0	10.9	576	11.07		-2.98	32.1	10.46	3.5

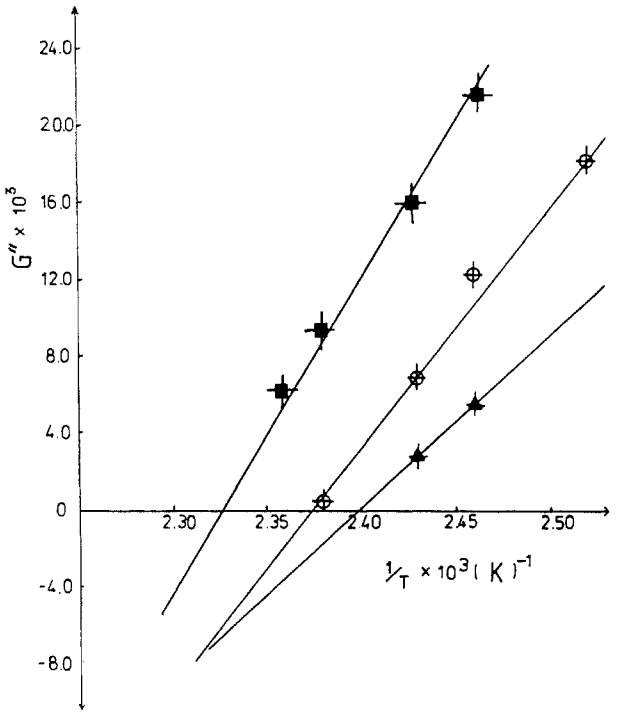

Figure 5. G''_i obtained from the forward scattered intensity from data as in Figure 4: ○, 26/74; ▲, 20/80; ■, 40/60.

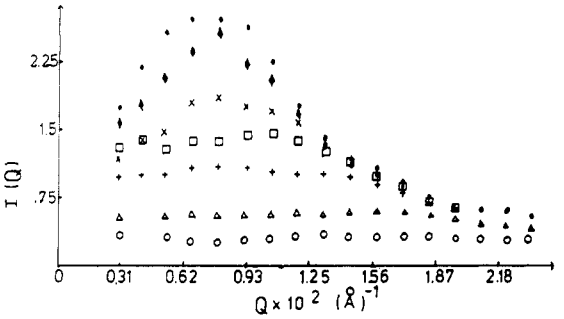

Figure 6. Normalized scattered intensity from a 26/74 blend after a temperature jump to within the spinodal. T = 154.0 °C. The curves are at 10 s intervals increasing in intensity with the first at 19 s after the jump.

and that the contribution of $S_T(Q)$ in eq 11 is negligible. This is in agreement with the results of Han et al.[10] who showed that $S_T(Q)$ only becomes important for very shallow quench depths (of the order of 1 K). In view of the subsequent discussion, it is worth noting that $I(Q)$ does not deviate much from linearity over the observed time scale.

From the initial slope of ln I vs t values of the growth rate $R(Q)$ can be obtained. In Figure 8 $R(Q)$ is shown as a function of Q for the data in Figure 6. A maximum is observed at Q_m as predicted by eq 9. Some temperature

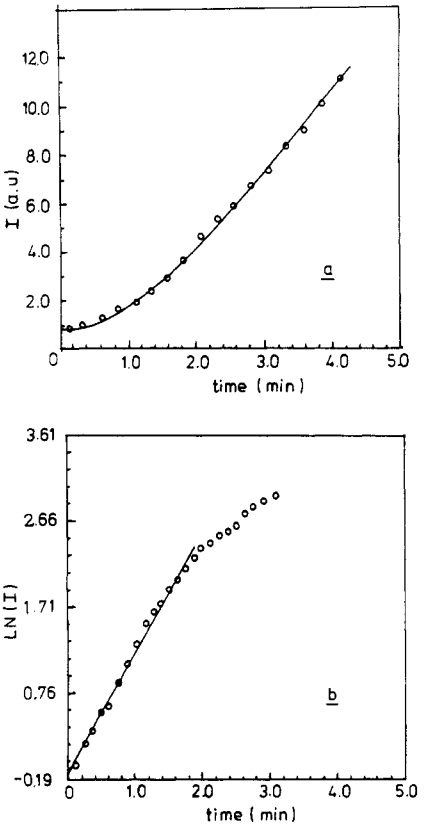

Figure 7. (a) Intensity against time at $Q = 6.3 \times 10^{-3}$ (Å^{-1}) for 26/74 blend at 154 °C. (b) ln I against time for the same mixture as in (a).

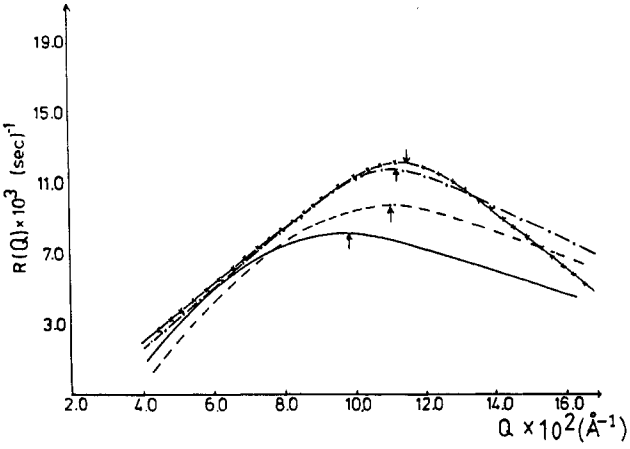

Figure 8. $R(Q)$ against Q for 26/74 blend at temperatures inside the spinodal: (—) 151.5 °C; (- - -) 153.0 °C; (-·-) 154.0 °C; (-×-) 155.0 °C.

dependence of Q_m can be seen from this diagram and more clearly from the values tabulated in Table III. The initial

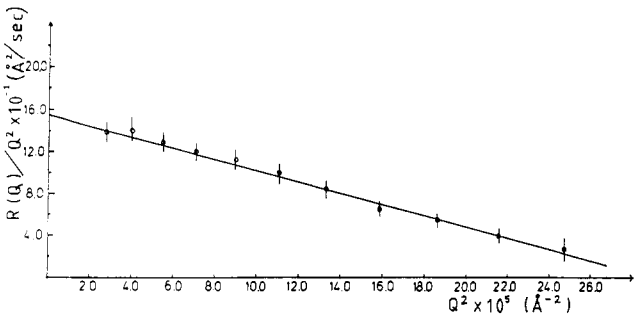

Figure 9. $R(Q)/Q^2$ against Q^2 for the mixture as in Figure 4 at 154.0 °C.

domain size is calculated as $d_0 = 2\pi/Q_m$.

The validity of the Cahn–Hilliard theory is also often tested via the linear dependence of $R(Q)/Q^2$ on Q^2 predicted by eq 7. For all the data reported here rather good linearity was observed within the experimental error, again supporting the interpretation of the data via Cahn–Hilliard theory. From the intercepts of plots such as shown in Figure 9 values of the Cahn–Hilliard diffusion coefficient ($\bar{D} = MG''_f$) are obtained and from the slopes values of $2MK$ (eq 7). Thus from the slope and intercept together, a second value of Q_m can be calculated, which gives an internal consistency check on the use of the Cahn–Hilliard theory to interpret the data. If eq 7 is obeyed, the values should be the same. These values are listed as Q'_m in Table III, where it is immediately obvious that while agreeing with Q_m in order of magnitude, they show for the 26/74 sample a reverse (weak) temperature dependence. This discrepancy with theory will be discussed below but must indicate small deviations from linearity, not observable within the errors in Figure 9.

As the thermodynamic driving force G'' decreases $\bar{D}$ should tend to zero at the spinodal. The values of $\bar{D}$ in Table III do show a weak temperature dependence but not nearly as strong a dependence as would be expected from their proximity to the cloud point obtained earlier. This could indicate either that the theory fails or that the cloud point is rather far from the true spinodal. We will return to this point in the subsequent discussion.

Given a value of the energy gradient parameter, K, it is possible to extract values of the thermodynamic term G''_f from Q_m via eq 8. The energy gradient parameter, K, was obtained in the random-phase approximation following eq 16 using literature values for R_g^2/M_w. For PMMA the ratio between R_g and $M_w^{1/2}$ was observed to be 0.26 in SANS experiments.[34] For PAMSAN there is no literature value available so the value of 0.25 for polystyrene was used.[35] Following the usual practice for scattering the z-average values of R_g were used. Clearly, there is a problem in the choice of parameters for substitution in eq 16 since it is not possible to rule out changes in conformation of either polymer within the blend. Such evidence as exists, however,[14,19] indicates that only small (<10%) perturbations in R_g occur in the blends. Within these uncertainties values of K listed in Table II allow values of G''_f to be calculated via eq 8. These values of G''_f are plotted together with G'' values from Figure 5 in Figure 10. Within the limits of accuracy already discussed, a good agreement can be observed between data obtained from either side of the spinodal. However the spinodal temperature T_{sp} is shifted a few degrees to lower temperatures than the cloud point. These spinodal temperatures are included with the cloud point value in Figure 2.

Equation 8 predicts that Q_m tends to zero at the spinodal. In order to test this relationship it is usual to express G''_f in terms of the quench depth $\Delta T = T - T_{sp}$

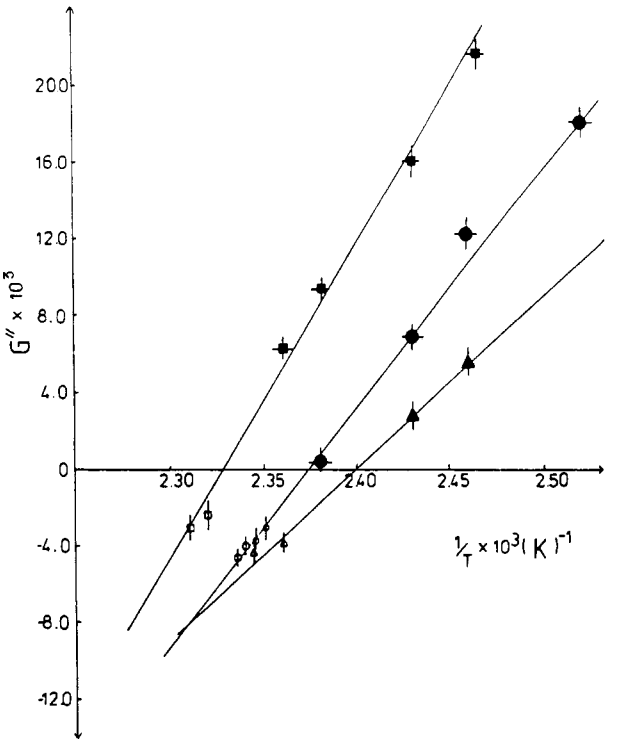

Figure 10. G'' vs T^{-1} combining data in Figure 5 with kinetic data in Table III, for blends: ●, 26/74; ▲, 20/80; ■, 40/60. Open symbols are values from Table II.

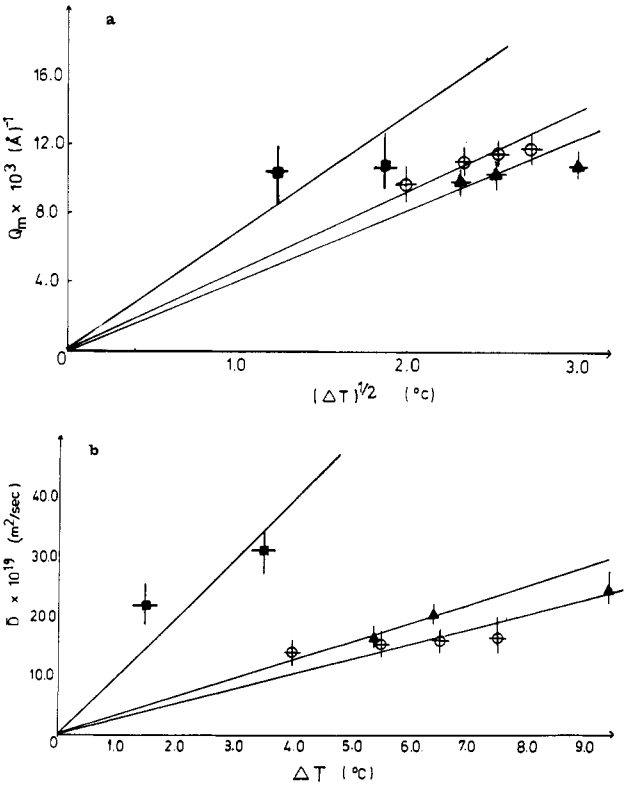

Figure 11. (a) Q_m vs $(\Delta T)^{1/2}$ for (⊙) 26/74, (▲) 20/80, and (■) 40/60. (b) $\bar{D}$ vs ΔT for (⊙) 26/74, (▲) 20/80, and (■) 40/60.

where T is the experimental temperature and T_{sp} the spinodal. Given the inverse temperature dependence of χ_{12} ($\equiv\alpha/T$), eq 2 becomes

$$G''_f = -2\alpha\frac{T - T_s}{T} = \frac{2\alpha}{T}\Delta T \qquad (17)$$

Thus for small ΔT where T varies very little, Q_m should vary as $\Delta T^{1/2}$. Figure 11a shows that the data do not really

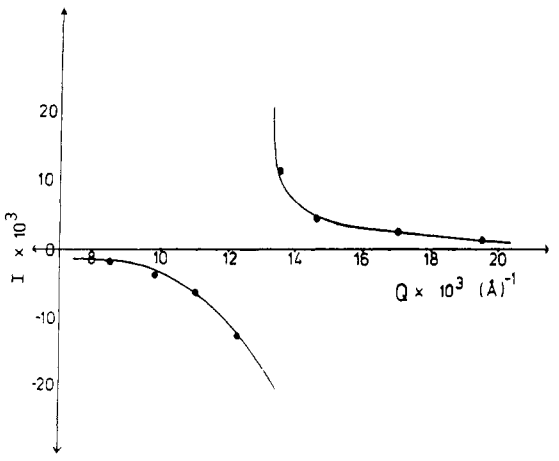

Figure 12. Virtual structure factor, $S_T(Q)$, as a function of wavevector, at 151.5 °C obtained by extrapolation of data in Figure 4 at each Q value vs T^{-1}.

follow the predicted behavior, showing a much flatter temperature dependence than given by eq 17.

Similarly, eq 10 predicts a linear dependence of $\bar{D}$ on ΔT, but Figure 11b again shows a much flatter variation than this prediction. Since the temperature dependence of M has been ignored, small deviations from linearity might be expected in Figure 11b. However, since M would be expected to increase with temperature, this would cause $\bar{D}$ to increase more rapidly than the effect of G''_f alone, and upward rather than downward deviations would be expected in Figure 11b.

Discussion

The predictions of the Cahn–Hilliard linearized theories can be summarized as follows: (1) Intensity increases exponentially with time with a growth rate of $2R(Q)$. (2) $I(Q)$ and $R(Q)$ have maxima at $Q_m = {}^1/_2(G''_f/K)^{1/2}$. (3) $R(Q)/Q^2$ varies linearly with Q^2. The intercept is $\bar{D} = MG''_f$, and the slope is $2KM$ so that $Q_m = {}^1/_2$(intercept/slope)$^{1/2}$. (4) The intensity does not grow above a cutoff $Q_c = 2^{1/2}Q_m$.

The data reported here are in quite good agreement with the first two of these predictions, but while $R(Q)/Q^2$ does apparently vary linearly with Q^2, values of Q_m obtained from slope and intercept neither agree with those observed directly in $R(Q)$ nor show the correct temperature dependence. Nor, moreover is $Q_c = 2^{1/2}Q_m$. Such discrepancies with the simple Cahn–Hilliard theory are usually attributed to ignoring the thermal fluctuation term $S_T(Q)$ in eq 12,[9,10,40] although Han et al.[10] suggest that $S_T(Q)$ will only be important for very small quench depths (of the order of 1 K). However, since "very small" may be a system dependent criterion, it is worth considering carefully the possible magnitude of the contribution of $S_T(Q)$. Now $S_T(Q)$ cannot be measured directly, but it can be obtained by extrapolating the data for $S(Q)$ from the one-phase region as demonstrated by Strobl et al.[36] using a parallel line shift of $S^{-1}(Q)$. The result of such an extrapolation of $S^{-1}(Q)$ against T^{-1} at each Q value to a temperature of 151.1 °C inside the spinodal for the 26/74 blend is shown in Figure 12.

The discontinuity in $S_T(Q)$ occurs at Q_c as can be seen from eq 3 when negative values of $S^{-1}(0)$ are inserted. Consideration of the value of Q_m given in Table III shows that Q_c in Figure 12 is approximately $2^{1/2}Q_m$.

The data in Figures 6 and 12 are presented on the same normalized scale to allow for comparison. The normalization of the two sets of data to an absolute scale, especially the very thin samples used in the kinetics experiments is not reliable, so the relative intensities in the figures may not be very accurately represented. Nevertheless, it seems clear that $S_T(Q)$ is not always negligible compared to $S(Q,0)$, especially for Q approaching Q_c.

In principle $S_T(Q)$, obtained by extrapolation in this way, could be used to analyze data according to eq 12; however, as already explained, it is difficult to normalize the two sets of experiments reliably, leading to over- or underestimate by 100%. Thus, it is worth considering in general the comparative values of $S(Q,0)$ and $S_T(Q)$. If the temperature jump were slow so that equilibrium was maintained, then $S(Q,0)$ would increase until the spinodal. At the spinodal G'' tends to zero, and hence $S(Q,0)$ tends to infinity, but $S(Q_m,0)$ has a finite value, which by substituting eq 8 in eq 3 with $G'' = 0$ is found to be $(-G''_f/2)^{-1}$. Similarly $S_T(Q)$ at Q_m is $(+G''_f/2)^{-1}$. Thus, $S(Q,0)$ and $S_T(Q)$ are always equal and opposite in value around Q_m in the limit that $S(Q,0)$ reflects scattering in the one-phase region close to the spinodal; this is true for any value of the quench depth. It is not possible to arbitrarily assume that for all but small quench depths $S_T(Q)$ is negligible. The relative importance of $S_T(Q)$ will depend on the exact magnitude of $S(Q,0)$ which will in turn depend both on sample preparation, equilibration before the temperature jump, and the rate at which the temperature jump is made. Carmesin et al.[38] explored the effect of a noninstantaneous temperature jump via computer simulations and found dramatic deviations from Cahn–Hilliard behavior, which included nonlinear $R(Q)/Q^2$ plots. The plots observed here are all linear, which may indicate that it is not the rate of temperature quenching that is causing the problem. It is more likely that it is the noninclusion of the thermal fluctuation term in the analysis that is causing the observed deviations from Cahn–Hilliard theory.

It is therefore important to consider more carefully the effect on the observed $R(Q)$ of using eq 9 to analyze data more correctly described by eq 12. Various authors, including Binder[6] and Snyder et al.,[37] have pointed out that because in the derivation of both eq 6 and 12 nonlinear terms in the diffusion equation were ignored, these equations represent an approximation that is only valid for $2R(Q)t < 1$. Examination of the values of $R(Q)$ presented in Figure 8 and the time scale used for the linear fit in parts a and b of Figure 7 shows that most of the data fall within this limit. In this case, only the leading terms in the exponential need be retained, leading to

$$S(Q,t) = S(Q,0)\left[1 + \left[1 - \frac{S_T(Q)}{S(Q,0)}\right]2R(Q)t\right] \quad (18)$$

The apparent growth rate $\hat{R}(Q)$ is then given by

$$\hat{R}(Q) = \left[1 - \frac{S_T(Q)}{S(Q,0)}\right]R(Q) \quad (19)$$

Thus a somewhat modified Q dependence of $R(Q)$ will be observed in practice.

Now, examination of Figures 7 and 12 shows that $S_T(Q)$ and $S(Q,0)$ are very flat over most of the Q range so that eq 19 predicts a small constant shift of $\hat{R}(Q)$ with respect to $R(Q)$. In fact the differences between $\hat{R}(Q)$ and $R(Q)$ only become significant around Q_c so it is not surprising that Q_c appears shifted. It is also reasonable that $\hat{R}(Q)$ shows a maximum close to the correct value at Q_m and that $\hat{R}(Q)/Q^2$ varies approximately linearly with Q^2. However, while $\bar{D}$ may be close to its correct value, the slope, which should be $2MK$, may be slightly altered so that the ratio of $\bar{D}$ to the slope would not correctly predict Q_m (as observed in practice in Table III). As is observed here in

Figure 11, the detailed dependence on G''_f (and hence quench depth) may be perturbed.

The correlation with the one-phase data shown in Figure 10 clearly indicates that the observed Q_m values are not markedly shifted by the $S_T(Q)$ term and thus that the linear Cahn–Hilliard theory is a good approximation to the data. The remarks above indicate that data for $Q < Q_m$ are less likely to be affected by ignoring the thermal fluctuation term. This is in agreement with a number of observations in the literature. Our own work[38] on phase separation in poly(ethylene vinyl acetate) copolymer/solution chlorinated polyethylene blends using light scattering showed good agreement with theory, but all the data were obtained for $Q < Q_m$. Strobl[36] on the other hand used small-angle X-ray scattering to study the polystyrene/poly(styrene-*co*-bromostyrene) blends. All his data are for $Q > Q_m$, and large effects of the thermal fluctuation terms were detected.

Figure 10 shows the first direct correlation between measurements of the free energy terms in the one- and two-phase regions. The overall agreement between data on either side of the spinodal is good and clearly indicates that the free energy terms on each side of the spinodal follow a mean-field variation.

In recent work using small-angle neutron scattering, Schwahn et al.[39] observed deviations from mean-field variation of G'' very close to the spinodal of a polystyrene/poly(vinyl methyl ether) blend. Those deviations lead to larger values of G'' in the range $\Delta T < 2$ K than would be obtained from extrapolation of values observed further from the spinodal. It would be of great interest to carry out kinetic measurements very close to the spinodal with careful temperature control and to combine these with measurements in the one-phase region in order to observe simultaneous deviations on either side of the spinodal within the critical region. Han et al.[10] worked within a quoted 0.05 °C of the spinodal in their kinetics measurements on a similar blend to Schwahn et al.[39] but report no deviations from mean-field behavior, though they do remark that the quench depth dependence of Q_m is incorrect. In the light of the above remarks this is a possible indication that they may have observed these critical effects.

Registry No. PAMSAN, 25747-74-4; PMMA, 9011-14-7; neutron, 12586-31-1.

References and Notes

(1) Cahn, J. W. *Trans. Metall Soc. AIME* **1986**, *242*, 169.
(2) Huston, E. L.; Cahn, J. W.; Hilliard, J. E. *Acta Metall.* **1966**, *14*, 1053.
(3) van Aartsen, J. J. *Eur. Polym. J.* **1970**, *6*, 919.
(4) Pincus, P. *J. Chem. Phys.* **1981**, *75*, 1996.
(5) de Gennes, P. G. *Macromolecules* **1979**, *9*, 587.
(6) Binder, K. *J. Chem. Phys.* **1983**, *79*, 6387.
(7) Schichtel, T. E.; Binder, K., in press.
(8) Hashimoto, T.; Kumaki, J.; Kawai, H. *Macromolecules* **1983**, *16*, 641.
(9) Snyder, H. L.; Meakin, P.; Reich, S. *Macromolecules* **1983**, *16*, 757.
(10) Okada, M.; Han, C. C. *J. Chem. Phys.* **1986**, *85*, 5317.
(11) Meier, H.; Strobl, G. R. *Macromolecules* **1987**, *20*, 649.
(12) Hill, R. G.; Tomlins, P. E.; Higgins, J. S. *Macromolecules* **1985**, *18*, 2556.
(13) Warner, M.; Higgins, J. S.; Carter, A. J. *Macromolecules* **1983**, *16*, 1931.
(14) Higgins, J. S.; Carter, A. J. *Macromolecules* **1984**, *17*, 2197.
(15) Tomlins, P. E.; Higgins, J. S. *Polymer* **1985**, *26*, 1554.
(16) Stein, R. S.; Hadziioannou, G. *Macromolecules* **1984**, *17*, 1059.
(17) Shibayama, M.; Yang, H.; Stein, R. S.; Han, C. C. *Macromolecules* **1985**, *18*, 2197.
(18) Lapp, A.; Picot, C.; Benoit, H. *Macromolecules* **1985**, *18*, 2437.
(19) Tomlins, P. E.; Higgins, J. S. *Macromolecules* **1988**, *21*, 425.
(20) Einstein, A. *Ann. Phys (Leipzig)* **1910**, *33*, 1275.
(21) Debye, P.; Beuche, A. *J. Chem. Phys.* **1950**, *18*, 1423.
(22) Flory, P. J. *J. Chem. Phys.* **1941**, *9*, 660.
(23) Cook, H. E. *Acta Metall.* **1970**, *18*, 297.
(24) Binder, K. *Phys. Rev. A* **1984**, *29*, 341.
(25) Eichinger, B.; Flory, P. J. *Trans. Faraday Soc.* **1968**, *14*, 2035.
(26) Flory, P. J.; Orwell, R. A.; Virug, A. *J. Am. Chem. Soc.* **1964**, 86.
(27) Jones, R. A. L. Ph.D. Thesis, Cambridge, 1987.
(28) Kramer, E. J.; Compasto, R. J. *Polym. Prepr. (Am. Chem. Soc., Div. Polym. Chem.)* **1987**, *28*, 323.
(29) Strobl, G. R. *Macromolecules* **1985**, *18*, 558.
(30) Carmesin, H. D.; Heerman, D. W.; Binder, K. *Z. Phys. B: Condens. Matter* **1986**, *65*, 89.
(31) Prentice, P. *J. Mater. Sci.* **1985**, *20*, 1445.
(32) Ibel, K. *J. Appl. Crystallogr.* **1976**, *9*, 396.
(33) Institut Laue-Langevin, Grenoble, France. For information contact the Scientific Secretariat.
(34) Dettenmaier, M.; Maconnachie, A.; Higgins, J. S.; Kausch, H. H.; Nguyen, T. Q. *Macromolecules* **1986**, *19*, 773.
(35) Wignall, G. D.; Ballard, G. D. H.; Schelten, J. *Eur. Polym. J.* **1974**, *10*, 861.
(36) Meier, H.; Strobl, G. R. *Macromolecules* **1987**, *20*, 649.
(37) Snyder, H. L.; Meakin, P. *J. Polym. Sci., Polym. Symp.* **1985**, *No. 73*, 217.
(38) Fernandez, M. L.; Higgins, J. S. Tomlins, P. E. *Polymer* **1989**, *30*, 3.
(39) Schwahn, D.; Mortensen, K.; Yee-Madeira, H. *Phys. Rev. Lett.* **1987**, *58*, 1544.